Numerical investigation of three wind turbine blade tips

Johansen, Jeppe; Sørensen, Niels N.

Publication date:
2002

Document Version
Publisher's PDF, also known as Version of record

Risø-R-1353(EN)

Numerical Investigation of Three Wind Turbine Blade Tips

Jeppe Johansen, Niels N. Sørensen

Risø National Laboratory, Roskilde
August 2002

Abstract The complex three-dimensional flow around three different tip shapes on a rotating wind turbine blade is investigated and analyzed using Computational Fluid Dynamics. Differences in production, flapwise bending moments and forces are discussed. A method for determining the local inflow angle of attack is presented and further analysis is performed on lift and drag coefficients.

It is shown that the original Standard tip results in a more concentrated tip vortex leading to a steeper gradient on both tangential and normal forces when approaching the tip, whereas the two tapered tips show a more flat behavior. This again leads to lower flapwise bending moments and lower production for the Standard tip compared to the two tapered tips. At 12 m/s, though, the Swept tip shows a separation pattern on the surface. This separation causes a decrease in normal force and an increase in tangential force. The Taper tip keeps the higher loading causing the flapwise bending moment to be higher as seen in measurements.

To determine the radial variation of lift and drag coefficients the local inflow angle of attack is determined. It is shown that the Standard tip experiences a slightly larger angle of attack at the tip compared to the two tapered tips. The lift coefficients are kept at a more constant level for the two tapered tips due to the decrease in chord, while the drag coefficients actually decrease for the two tapered tips, especially for the Swept tip. For the Swept tip at 12 m/s both lift and drag coefficients changed considerably due to the separation

Differences in aerodynamic damping of the three tips were investigated using HAWCDAMP. The Standard tip seems to be slightly less damped with respect to the flapwise vibrations, but no particular differences were obtained with respect to the edgewise vibrations.

Front picture shows streamlines around three tips and iso-vorticity surfaces downstream

ISBN 87-550-3087-4; ISBN 87-550-3088-2 (Internet)
ISSN 0106-2840

Print: Pitney Bowes Management Services Denmark A/S, 2002

Contents

1 Introduction

It is well known that the geometry of a rotor tip influences the aerodynamic damping [1] and aeroacoustics [2] of a wind turbine rotor. But for the overall aerodynamics of the rotor the influence of the tip is not well investigated. The flow around the tip is a very complex three-dimensional flow and the present design and analysis tools used for blade design do not resolve the details of the flow. As a consequence this causes tip design to be based mainly on simple engineering methods, such as e.g. Blade Element Momentum methods, experiments, experience and intuition. Many experiments have been carried out to investigate tip flows. But, to the authors' knowledge, the only experiment where several tips have been measured on the same wind turbine rotor is the one described in Antoniou et al [3]. Here a 95 kW Tellus wind turbine with LM8.2 blades has been equipped with five different tips in order to investigate the influence on rotor performance.

The purpose of the present work is to apply Computational Fluid Dynamics, CFD, to validate and supplement the conclusions made in the experimental work. Using CFD it is possible to resolve the complex flow around the tip and through analysis gain a better understanding of the flow physics. This will eventually help in developing more physically correct design guidelines for wind turbine blade tips. Section 2 describes the work, where three of the five different tips were chosen from the Tellus experiment and focus is made on the low wind speeds, where the flow is mostly attached and where CFD is known to give reasonable predictions.

Also the aerodynamic damping of the three different tips is investigated and described in Section 3. Only the first flapwise and edgewise damping modes have been investigated. Finally Conclusions are drawn in Section 4.

2 Aerodynamics of wind turbine blade tips

The three tips investigated in the present study are shown in Figure 1. They are the Standard tip, the Swept tip (which is also tapered) and the Taper tip.

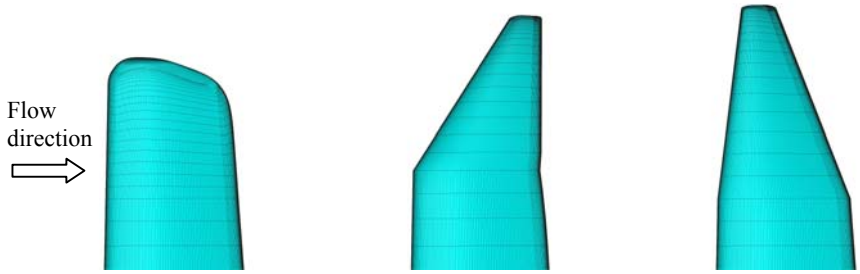

Figure 1: Three tips from the Tellus 95 kW wind turbine: Standard (left), Swept (middle) and Taper tip (right), respectively. The leading edge is to the left.

2.1 Method

The CFD code EllipSys3D is used for the present investigation. The code is developed by Michelsen [4], [5] and Sørensen [6] and is a multiblock finite volume discretization of the incompressible Reynolds Averaged Navier-Stokes equations in general curvilinear coordinates. The code uses a collocated variable arrangement, and Rhie/Chow interpolation is used to avoid odd/even pressure decoupling. As the code solves the incompressible flow equations, no equation of state exists for the pressure and the SIMPLE algorithm is used to enforce the pressure/velocity coupling. The EllipSys3D code is parallelized with MPI for executions on distributed memory machines, using a non-overlapping domain decomposition technique. Solution of the momentum equations is obtained using a second order upwind differencing scheme (SUDS) for the convective terms. Computations are made assuming steady state conditions taking advantage of a local time stepping algorithm. Computations are performed assuming fully turbulent flow and the turbulent eddy viscosity is modeled using the k-ω SST model by Menter [7].

Computations are performed on the rotor only neglecting tower and nacelle and the computational grids are made using an in-house hyperbolic grid generator, HypGrid3D. The grid consists of two regions: The inner region around the blade consists of five blocks with 64^3 cells in each. There are 256 cells around the blade in the chordwise direction and 64 in the spanwise direction. At the tip an additional block of 64x64 cells is placed. The number of cells in the normal direction away from the surface is 64. An outer region consisting of three blocks of 64^3 cells is wrapped around the inner region. This gives in total $2.1 \cdot 10^6$ grid cells.

The outer boundary of the computational domain is spherical and located approximately five rotor diameters away. On the blade surface a no-slip boundary condition is used. On the inner surface surrounding the rotational axis a slip boundary condition is applied. The outer boundary has inflow and outflow boundary conditions, respectively. See Figure 2.

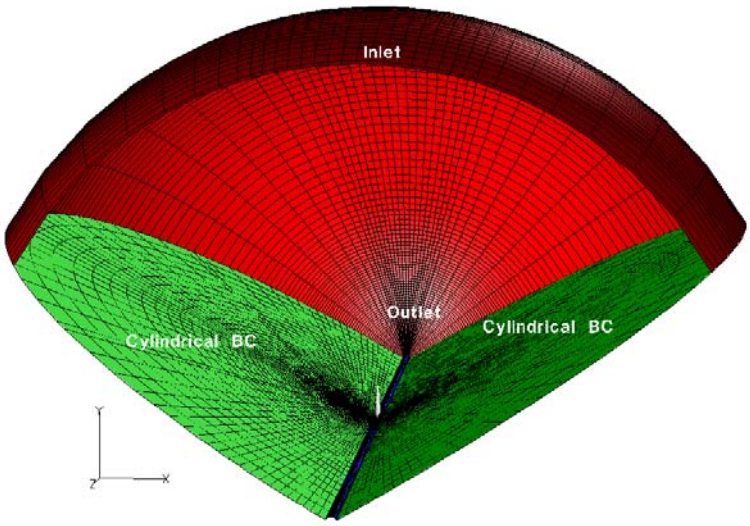

Figure 2: Computational grid around the LM8.2 blade equipped with a Standard tip.

2.2 Results

Computations have been made on the rotor of a 95 kW Tellus wind turbine equipped with three LM8.2 blades on a 1.3 m extender. Wind speeds varying from 7 m/s to 20 m/s have been computed for all three tips, but focus will mainly be put on the low wind speeds, i.e. 7, 10 and 12 m/s, where the agreement with measurements is good. The rotational speed is 47.9 rpm corresponding to $\Omega = 5.016$ rad/s. The pitch angle at the blade tip is 1.8°. In the experiment the rotor is tilted 5°, but this is not accounted for in the present computations.

Results are presented as power production, flapwise bending moments, radial force distributions and flow visualization. A method of determining the local inflow angle of attack will be presented and lift and drag coefficients will be extracted.

Production

Figure 3 shows the computed mechanical power compared with the measured mechanical power. It is seen that there is a considerable over prediction at peak power, which is a well-known problem. Some of the main reasons are incorrectly prediction of the flow separation and transport of turbulence using a conventional two-equation RANS turbulence model. The neglect of transition from laminar to turbulent flow is also believed to influence the power prediction. At low wind speeds, though, the agreement is good.

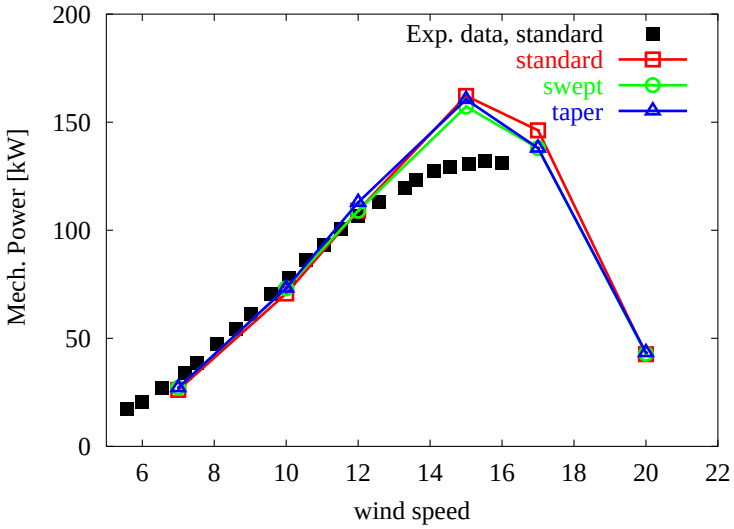

Figure 3: Computed power for the three tips compared with measured power for the Standard tip.

Flapwise bending moments

Figure 4 show the flapwise bending moments for the three different tips

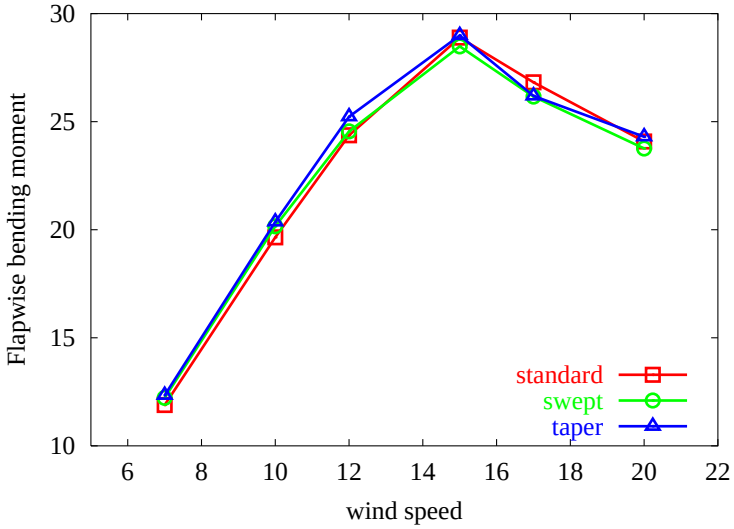

Figure 4: Computed flapwise bending moment for the three tips

There is no large difference in the computed flapwise moments, but at around 12 m/s the flapwise bending moment for the Taper tip is slightly larger compared to the two other tips.

Radial force distributions

To further investigate this, the tangential, or driving, force, F_x, and normal force, F_z, distributions have been plotted for the outer 1.7 m of the 10 and 12 m/s case, Figure 5. (7 m/s behaves similar to the 10 m/s case.)

First it should be noted that the plane area is kept constant for the three blades causing the Standard tip to be shorter than the two tapered tips. The Standard tip shows a steeper gradient on both tangential and normal force when approaching the tip. This indicates that the circulation decreases more abruptly, and the tip

vortex generated by the Standard tip is more concentrated compared to the two other tips. Secondly, it can be deduced that the two tapered tips have a slightly larger loading at the tip indicating that a tapered tip is more efficient based on power production at low wind speeds.

At 12 m/s (up to approx. r = 9.5 m) the Swept tip shows a steeper decrease in force distribution similar to the Standard tip. The flattening of the force distribution is caused by a separation of the flow. The force distribution of the Taper tip decreases more gradually, which explains the previously mentioned higher value of flapwise bending moment for the Taper tip. This is also seen in the measurements. (The discontinuity at r = 9.1 m on the Swept tip is caused by the discontinuity in the geometry as seen in Figure 1)

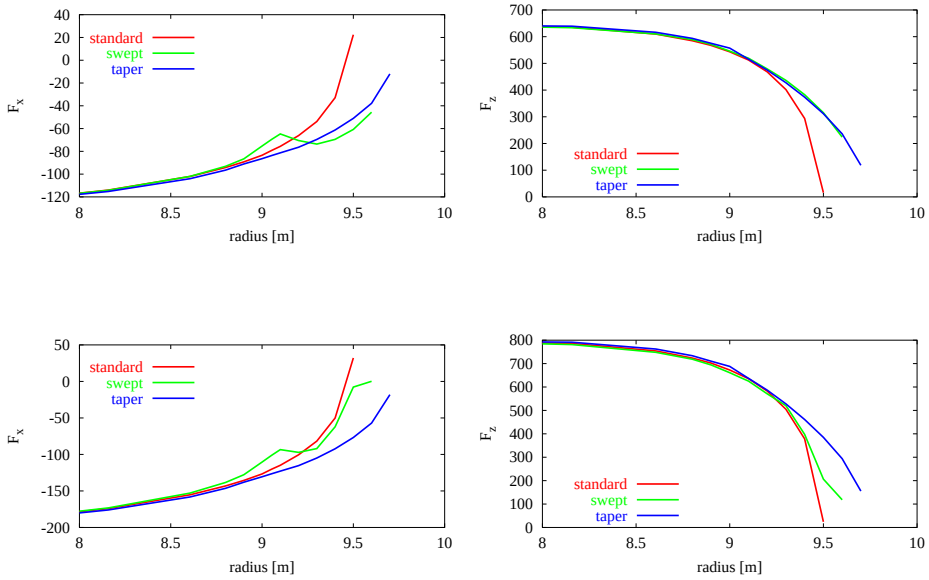

Figure 5: Radial tangential and normal force distributions for 10 m/s (top) and 12 m/s (bottom), respectively. The discontinuity seen on the Swept tangential force at 9.1 m is caused by a discontinuity on the blade geometry (See Figure 6).

Flow visualization

By looking at limiting streamline plots, Figure 6, it is observed that the decrease in force distribution from 10 to 12 m/s for the Swept tip is due to a flow separation close to the tip. This separation is probably caused by a combination of decrease in chord, resulting in a lower Reynolds number, and the sweep of the leading edge.

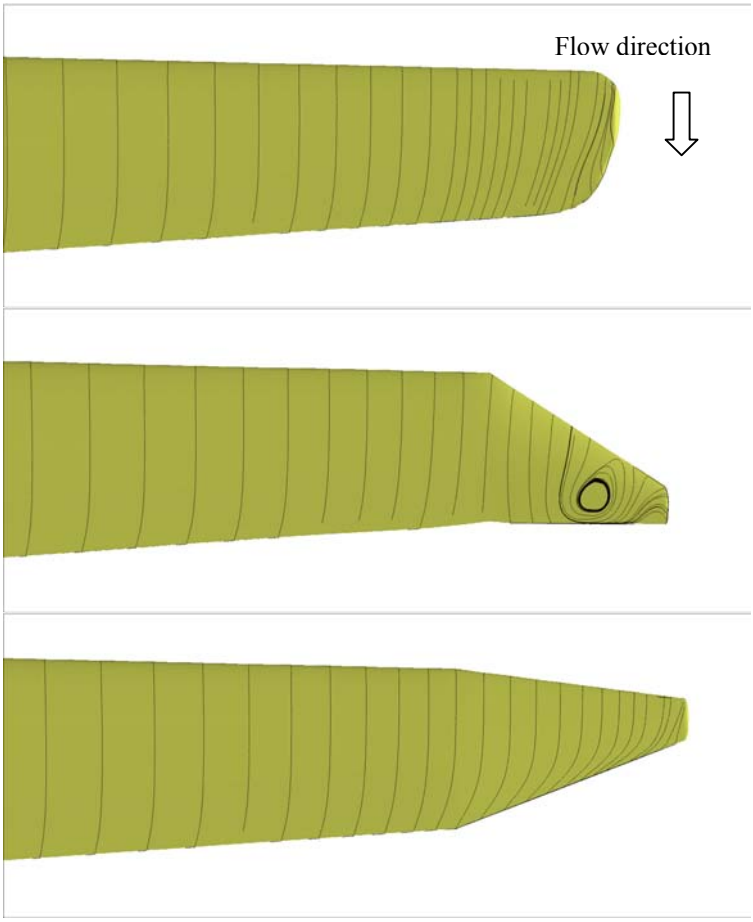

Figure 6: Limiting streamlines at W=12 m/s of the outer part of the blades with Standard (top), Swept (middle) and Taper (bottom) tip, respectively.

At 15 m/s the same kind of separation is appearing on the Taper tip, even though the size of the vortex is not as large compared to the one on the Swept tip. The Standard tip does not show such a separation pattern on the surface.

Figure 7 shows streamlines around the tip region of the three blades. The flow is coming from left to right. Approximately one meter downstream an iso-vorticity surface is shown to display the spatial extension of the shed vorticity. It is seen that the dark center of the tip vortex is slightly larger on the Standard tip indicating a more concentrated tip vortex, whereas the vorticity for the two tapered tips are more "smeared" out. The pressure contours on the blades show a regular pattern except on the outer part of the Swept tip, where the separated region is seen as a constant pressure plateau.

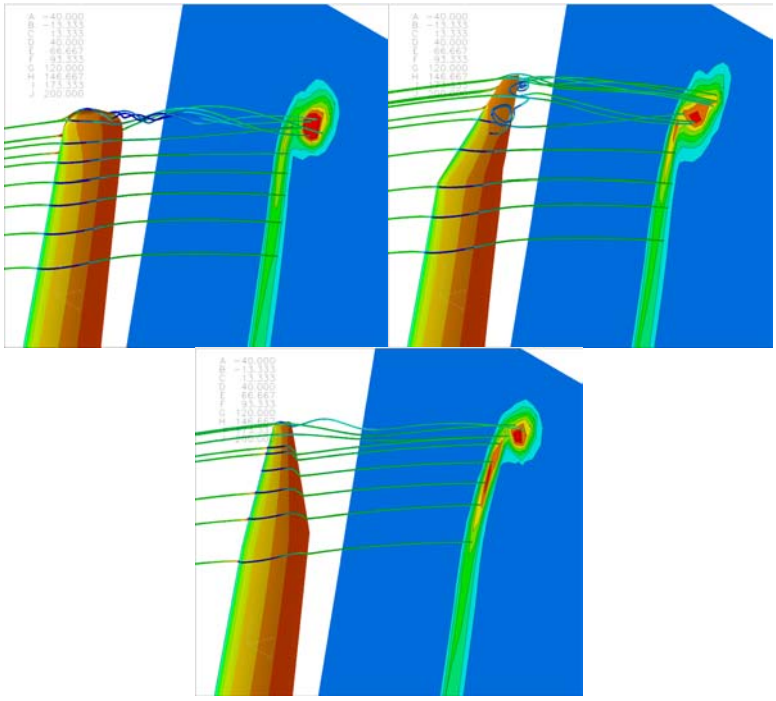

Figure 7: Streamlines around the three tips and iso-vorticity surfaces downstream showing the spatial extension of the tip vortex. W = 12m/s.

Reynolds Number

A second reason for the Standard tip not to separate could be the local Reynolds number, which decreases as the chord decreases. Figure 8 shows the local Reynolds number as function of radius, and it is seen that for the two tapered tips the Reynolds number decreases to around $5 \cdot 10^5$. At this Reynolds number the transition from laminar to turbulent flow is known to have a large influence on the flow.

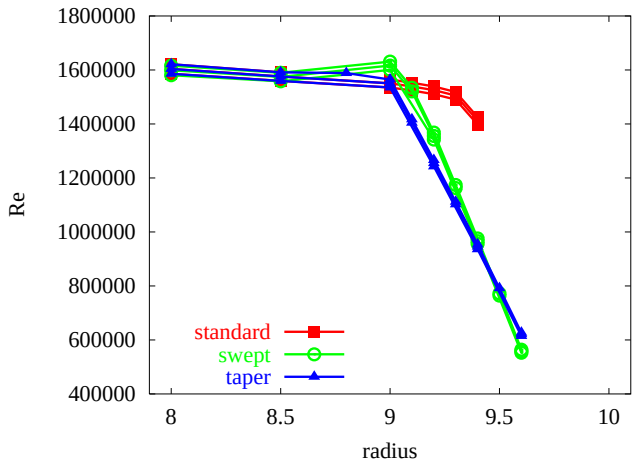

Figure 8: Local Reynolds number as function of radius. For wind speeds = 7, 10 and 12 m/s.

Angle of attack

To further investigate the local flow around the various tips it is convenient to define the local angle of attack. It is well known that the actual incidence of the flow around a wing or blade is difficult to define due to induced velocities from

the blade. Here we will present a method of determining this local angle of attack, α_{inflow}. The method is based on determining the disturbed axial velocity and is called *the reduced axial velocity method*.

The method is a way to determine the actual inflow velocity taking into account the decrease in axial flow due to the presence of the rotor. In the reduced axial velocity method the average incoming axial velocity is determined in a thin annular element at a specific radial position in consideration (See Figure 9). The reduced axial velocity as function of axial position can be obtained by sweeping this annular element from upstream to downstream the rotor in the axial direction, Figure 10. Now the reduced axial velocity in the rotor plane can be determined (axial position = 0 in Figure 10). Knowing the rotational speed and the local pitch setting it is now possible to determine the local angle of attack.

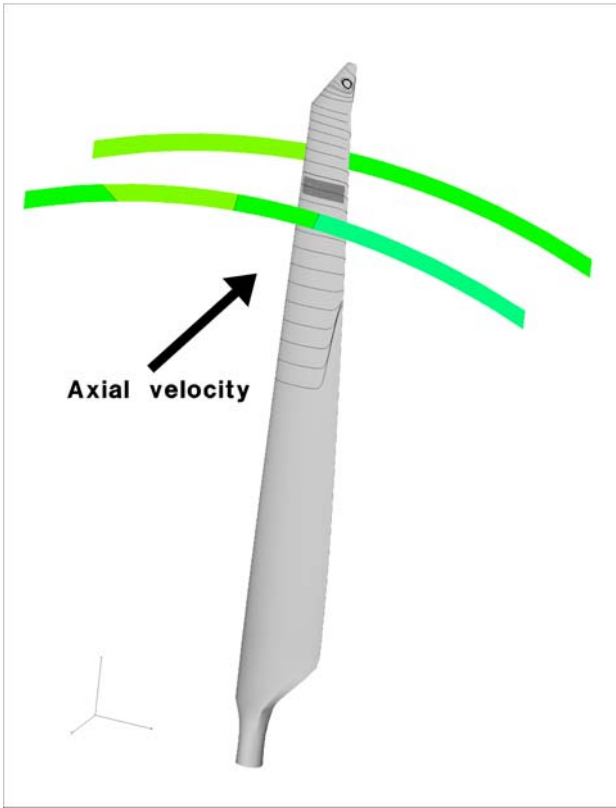

Figure 9: Schematic plot showing the principle of the reduced axial velocity method. The thin annular element is placed at radius = 8.16 m.

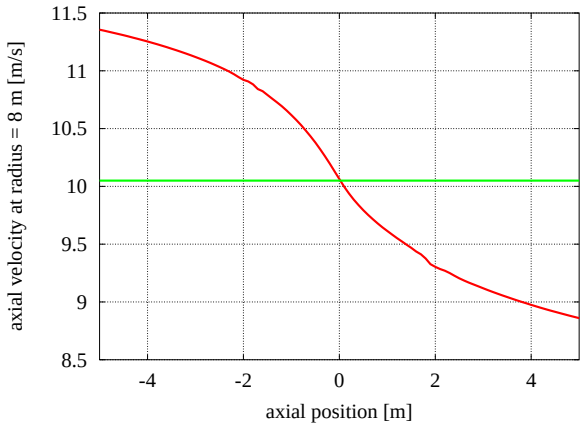

Figure 10: Averaged axial velocity as function of axial position at radius = 8.16 m.

In order to check or validate the angle of attack, 2D computations are performed around this angles of attack on an airfoil section with the same physical dimension, grid point distribution and Reynolds number as the 3D case. By comparing the 2D stagnation point location and pressure distribution with the 3D pressure distribution it is possible to determine the "correct" corresponding angle of attack.

The method is illustrated in the following example.

Blade	LM8.2 with a 1.3 m extender and a Swept tip
Rpm, Ω:	5.016 rad/s
Radial position, r	8.16 m
Wind speed, W	12 m/s
Blade pitch, α_{pitch}	-0.6°

Using the reduced axial velocity method at radius = 8.16 m one gets an axial velocity of 10.05 m/s (Figure 10), which corresponds to an angle of attack,

$$\alpha_{inflow} = \arctan\left(\frac{w}{r\Omega}\right) + \alpha_{pitch} = \arctan\left(\frac{10.05}{8.16 \cdot 5.016}\right) - 0.6° = 13.2° \, .$$

Three 2D angles of attack have been computed around 13.2° and Figure 11 shows (top) the 2D pressure distributions compared with the 3D pressure distribution. A close up around the stagnation point is shown at the bottom.

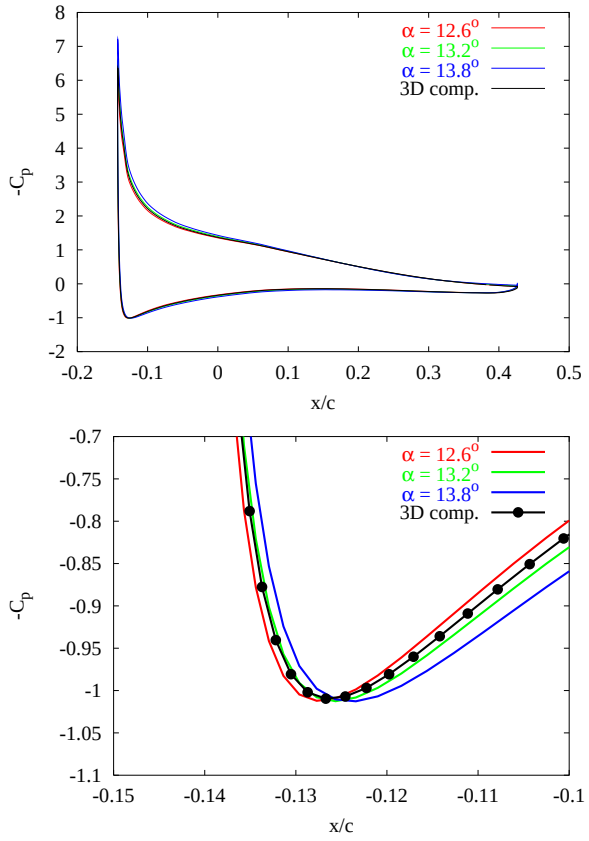

Figure 11: Three 2D pressure distributions compared with a 3D pressure distribution.

First it is seen that the 3D pressure distribution has same shape as the 2D pressure distributions indicating that the flow at this particular radial position is very close to being 2D. Secondly, one observes that the best agreement is obtained with the 2D computation at 13.2° as predicted by the reduced axial velocity method.

The local inflow angle of attack has been computed using the reduced axial velocity method for the outer part of the blades, even though the method is questionable close to the tip due to three-dimensional effects. Also at high angles of attack, where the flow separates, it can be difficult to determine a corresponding 2D angle of attack.

Figure 12 and Figure 13 show the variation of reduced axial velocity, w, and local inflow, $\alpha_{inflow,}$ respectively, as function of radial position of the three different tips. (The local blade pitch setting only varies from -0.7° at 8.0 m radius to -0.2° at the tip). The plots are grouped according to wind speed. The top three curves correspond to 12 m/s, the middle three curves correspond to 10 m/s and the bottom three curves correspond to 7 m/s.

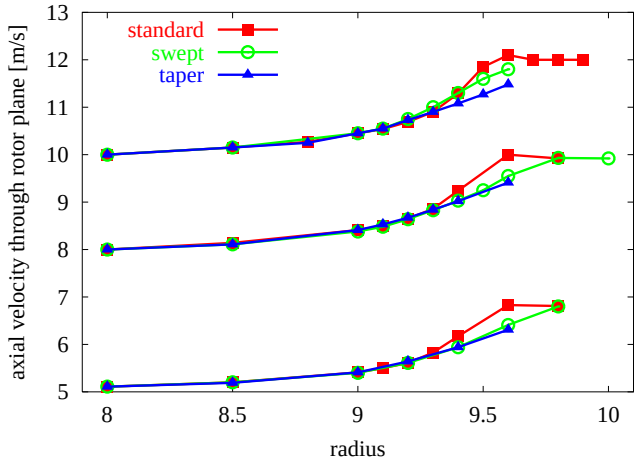

Figure 12: Variation of axial velocity in the rotor plane for three different tips at three different wind speeds.

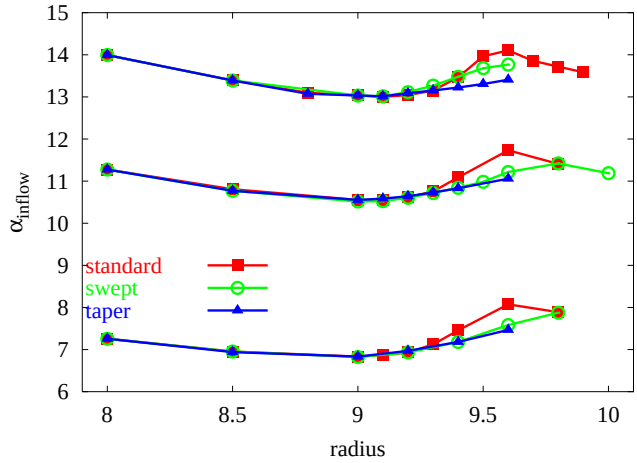

Figure 13: Variation of inflow angle of attack for three different tips at three different wind speeds.

It is seen that there is no difference in axial velocity and therefore in angle of attack between the different tips at radius < 9.2 m. But at around 9.5 m radius (right at the tip!) the Standard tip shows an angle of attack, which is around 0.5° larger than the Swept tip, which again is 0.5° larger than the Taper tip for 12 m/s. This could also influence the later separation of the Taper tip compared to the Swept tip.

Lift and drag coefficients

Now that we have both forces and angles of attack it is possible to determine the lift and drag curves at the tip by

$$L = F_z \cos \alpha_{inflow} - F_x \sin \alpha_{inflow}$$

and

$$D = F_z \sin \alpha_{inflow} + F_x \cos \alpha_{inflow}.$$

Figure 14 shows the lift and drag coefficients as function of radius for the three tips at three different wind speeds.

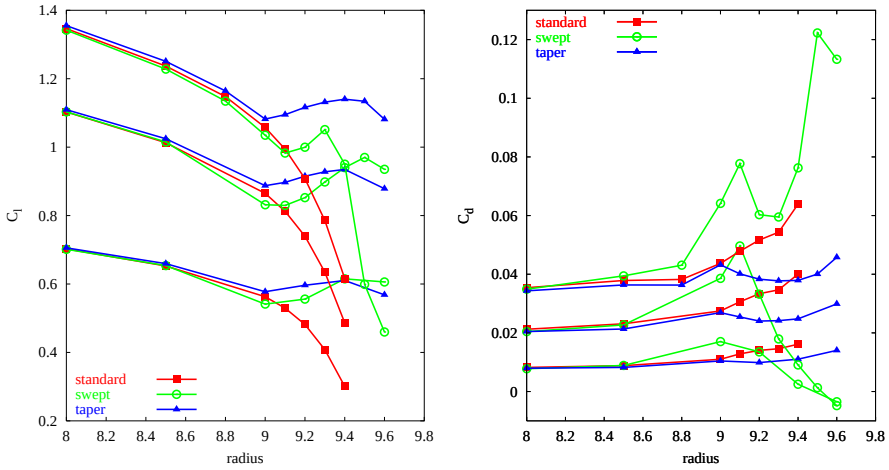

Figure 14: Lift and drag coefficients as function of radius for the three different tips at three different wind speeds.

Several aspects can be observed in the plots. Starting with the three 7 m/s curves in Figure 14 it is seen that the lift coefficient for the Standard tip is decreasing approaching the tip, while the two tapered tips are kept approximately constant. This is mainly due to the smaller aspect ratio for the Standard tip. Also the slope of the decrease increases with radius, which indicates that three-dimensional effects are more pronounced for the Standard tip compared to the two tapered tips. For the Swept tip the drag coefficient are slightly increasing until the point where the swept tapering begins. After that, drag is decreasing and even becomes negative at the tip. This is caused by a combination of the decrease in chord and an even larger decrease in drag force. Also the determination of inflow angle of attack could be questionable due to 3D effects. A similar but weaker effect is seen for the Taper tip. At 10 m/s the trends are more pronounced.

Finally, at 12 m/s the flow on the Swept tip separates at the tip, which causes the lift to decrease and the drag to increase.

3 Aerodynamic damping

The second aspect considered in the present report is the investigation of the aerodynamic damping of the blade equipped with the three different tips.

At high winds stall regulated wind turbines do in some cases experience undesirable unstable vibrations, called stall induced vibrations. This phenomenon is associated with the amount of total damping of the turbine. The total damping consists of the structural damping and of aerodynamic damping. The latter is highly dependent on wind speed. In some cases negative aerodynamic damping exceeds the positive structural damping resulting in a total damping being negative, which again causes the wind turbine to vibrate in an unstable condition.

Aerodynamic damping for a given airfoil section is defined as the integration over one cycle of the work, $\vec{F}_i\vec{v}$, performed by the aerodynamic forces on the blade structure in a simple harmonic motion.

$$W_i = \int_o^T \vec{F}_i \vec{v} dt$$

Here $\vec{F}_i$ is the force in the edgewise (x) and flapwise (y) directions, respectively, $\vec{v}$ is the velocity of the airfoil section, t is time and T is the period of the oscillating motion.

The aerodynamic damping is positive when the work performed by the aerodynamic forces is negative.

The stability of the system is defined by the logarithmic decrement of the local modal damping along the blade, $\delta(r)$, defined as

$$\delta(r) = \ln \frac{A_t}{A_{t+T}}, \quad T = \frac{2\pi}{\omega},$$

where A_t is the amplitude of vibration at time t. Finally, the local modal damping can be integrated over the length of the blade to give the global modal damping:

$$\delta = \int_{blade} \delta(r) dr \, .$$

3.1 Method

The modal damping is computed using HAWCDAMP [8], which is a commercial software developed at Risø National Laboratory for computing and analyzing the aerodynamic damping of a wind turbine blade.

The aerodynamic model in HAWCDAMP is based on the Blade Element Momentum (BEM) theory. As input to the model airfoil characteristics are needed. In the present work these has been extracted from the CFD computations described in the previous chapter.

The extracted lift and drag coefficients, C_l and C_d, for the Standard tip, Swept tip and Taper tip, respectively, are shown as function of angle of attack, α, in Figure 15 to Figure 17.

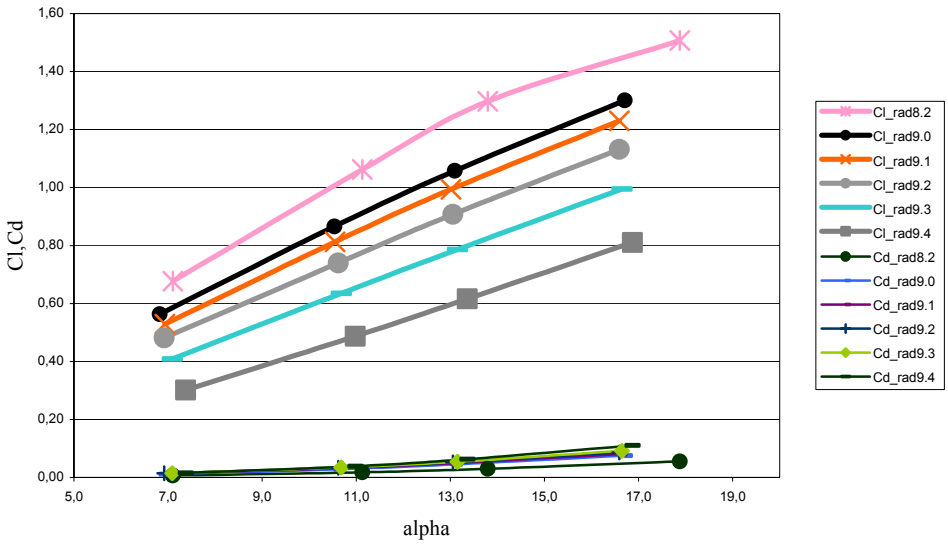

Figure 15: Lift and drag data extracted from CFD computations (Standard tip)

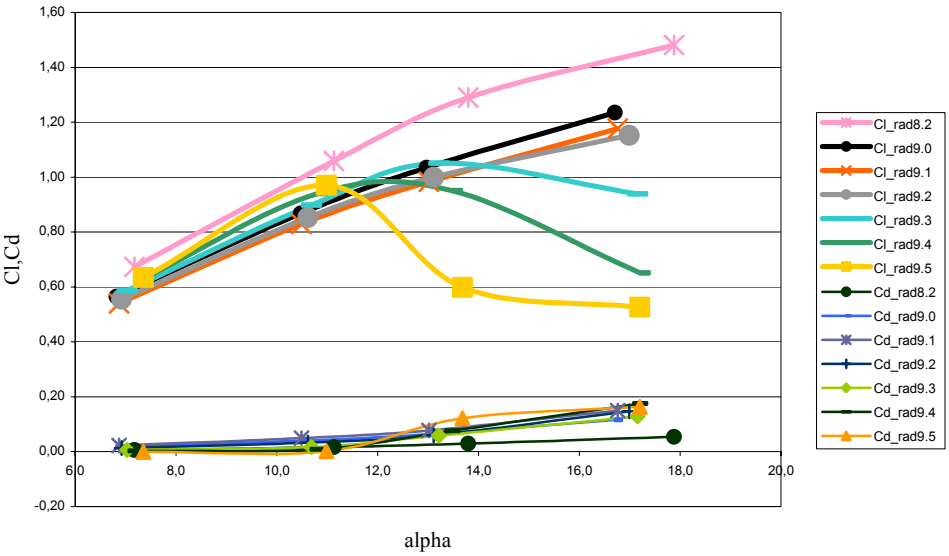

Figure 16: Lift and drag data extracted from CFD computations (Swept tip)

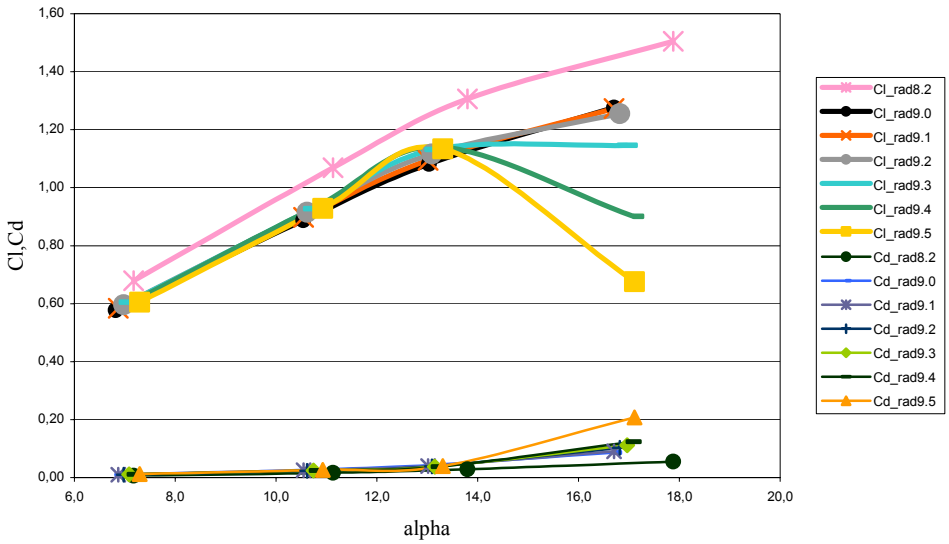

Figure 17: Lift and drag data extracted from CFD computations (Taper tip)

Only the outer 1.3 m of the blade is shown and only 7, 10, 12 and 15 m/s are used for extracting airfoil characteristics. The lift coefficient of the Standard tip shows a decrease in both C_l and C_l-slope approaching the tip. The two tapered tips shows a more constant C_l level at lower angles of attack whereas the flow separates earlier when approaching the tip.

3.2 Results

Production

The resulting power curves using HAWCDAMP are shown in Figure 18 and Figure 19.

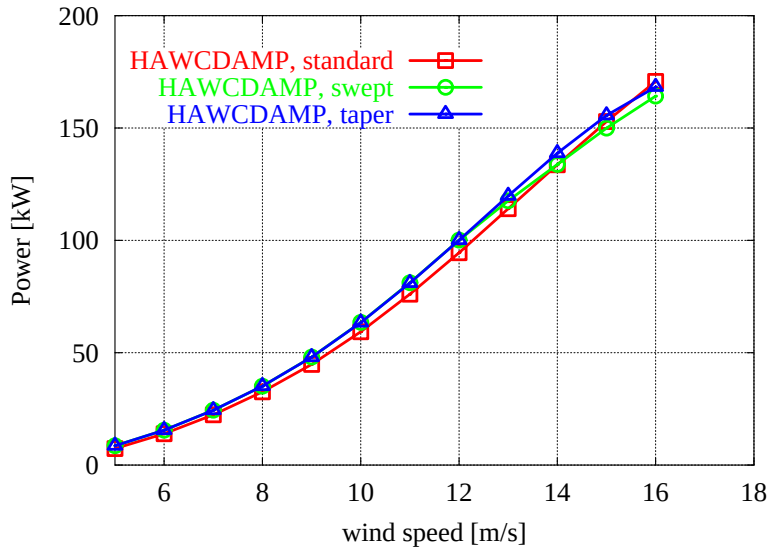

Figure 18: Power curve from HAWCDAMP.

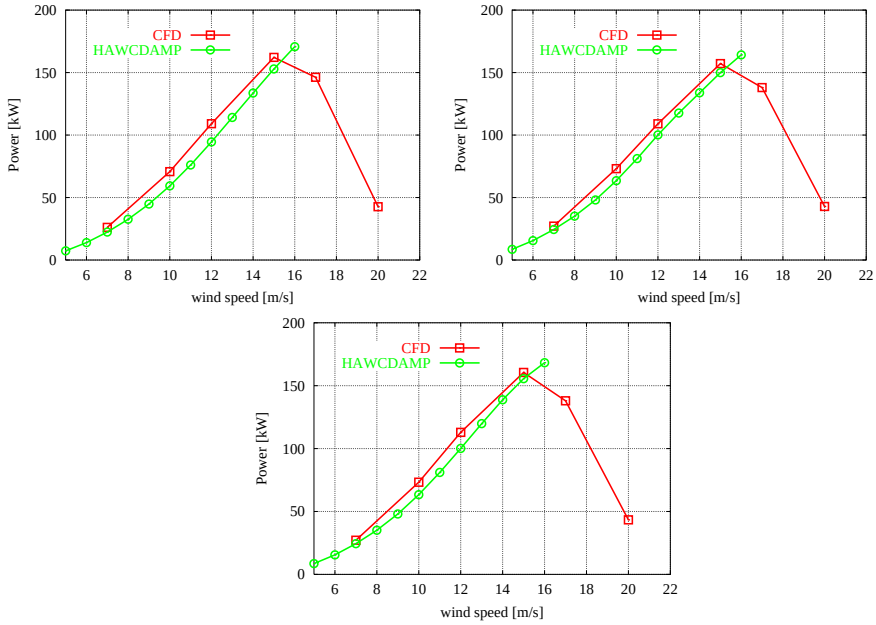

Figure 19: Power curves for Standard tip, Swept tip and Taper tip, respectively. Both CFD and HAWCDAMP

It is seen from Figure 19 that the HAWCDAMP power curves are in relatively good agreement with the CFD predictions indicating that the method of extracting the corresponding inflow angle of attack is reasonable. The extracted data does automatically take into account rotational effects together with 3D effects. It is thus not necessary with further 3D corrections.

For the aerodynamic damping calculations only the to first flapwise and edgewise mode shapes are used. These have been computed using the finite element program HAWC and are shown in Table 1.

Table 1: Normalized flapwise and edgewise mode shapes of the LM8.2 blade with Standard tip.

	1. flapwise mode (f=2.53 Hz)		1. edgewise mode (f=5.58Hz)	
Radius [m]	x-defl. [-]	y-defl. [-]	x-defl. [-]	y-defl. [-]
0.000	0.00	0.00	0.00	0.00
2.575	$-1.70\cdot10^{-4}$	$3.54\cdot10^{-3}$	$3.96\cdot10^{-2}$	$-9.86\cdot10^{-2}$
6.580	$4.62\cdot10^{-2}$	$4.25\cdot10^{-1}$	$4.84\cdot10^{-1}$	$7.38\cdot10^{-2}$
7.080	$5.56\cdot10^{-2}$	$5.13\cdot10^{-1}$	$5.54\cdot10^{-1}$	$1.02\cdot10^{-1}$
8.113	$7.52\cdot10^{-2}$	$7.14\cdot10^{-1}$	$7.24\cdot10^{-1}$	$3.46\cdot10^{-2}$
9.500	$1.01\cdot10^{-1}$	1.00	1.00	$-1.83\cdot10^{-1}$

The mode shapes are computed for the LM8.2 blade with the Standard tip and are used for the two other tips as well.

Computations using HAWCDAMP have been performed using both the Stig Øye dynamic stall model and the Beddoes-Leishman dynamic stall model for the unsteady aerodynamics. The aerodynamic damping is determined by moving the blade according to the given mode shape with a given amplitude, in this case 20 cm in both the flapwise and the edgewise direction. The number of blade elements in the HAWCDAMP computation is 12.

First flapwise mode shape

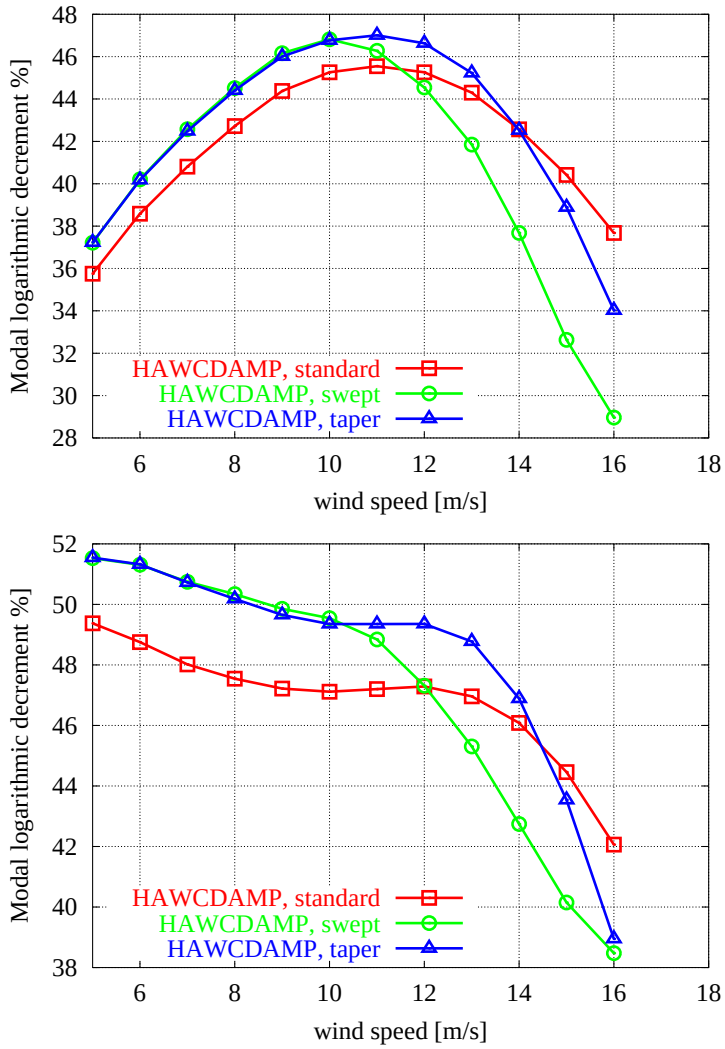

Figure 20: Computations of global modal damping of the three different tips excited in first flapwise mode shape using HAWCDAMP with Stig Øye model (top) and Beddoes-Leishman model (bottom)

The global modal damping, or the modal logarithmic decrement, in flapwise direction is shown in Figure 20 and it can be seen that damping is positive for all wind speeds. Despite the differences using different dynamic stall models it is seen that the Standard tip are slightly less stable at low wind speeds, while the Swept tip is slightly less stable at higher wind speeds.

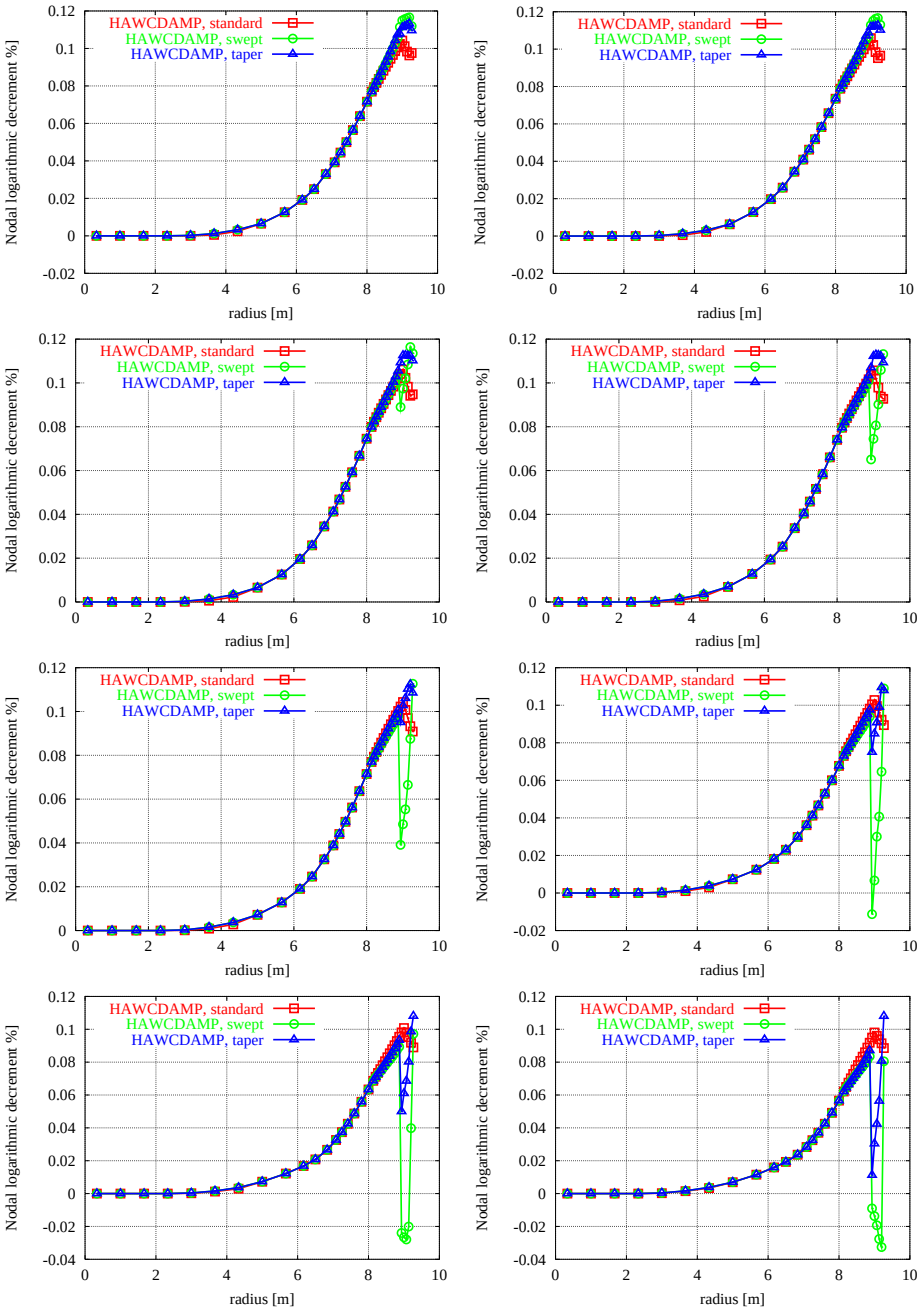

Figure 21: Local modal damping for 9, 10, 11, 12, 13, 14, 15 and 16 m/s, respectively, when first flapwise mode shape is excited (Stig Øye model).

By looking at the radial distribution of the local modal damping, or nodal logarithmic decrement, Figure 21, it is seen that the difference in damping at high winds for the Swept tip is caused by the earlier separation. Due to this separation the slope of the C_l-curve is negative causing the aerodynamic damping to become negative. The Taper tip experiences a comparable behavior at the higher wind speeds but not as severe.

First edgewise mode shape

The global modal damping in edgewise direction is shown in Figure 22 and it is seen that damping is positive up till around 13 m/s using the Stig Øye model, while the global modal damping changes sign at around 9.5 m/s using the Beddoes-Leishman model. The difference between the tips is very small.

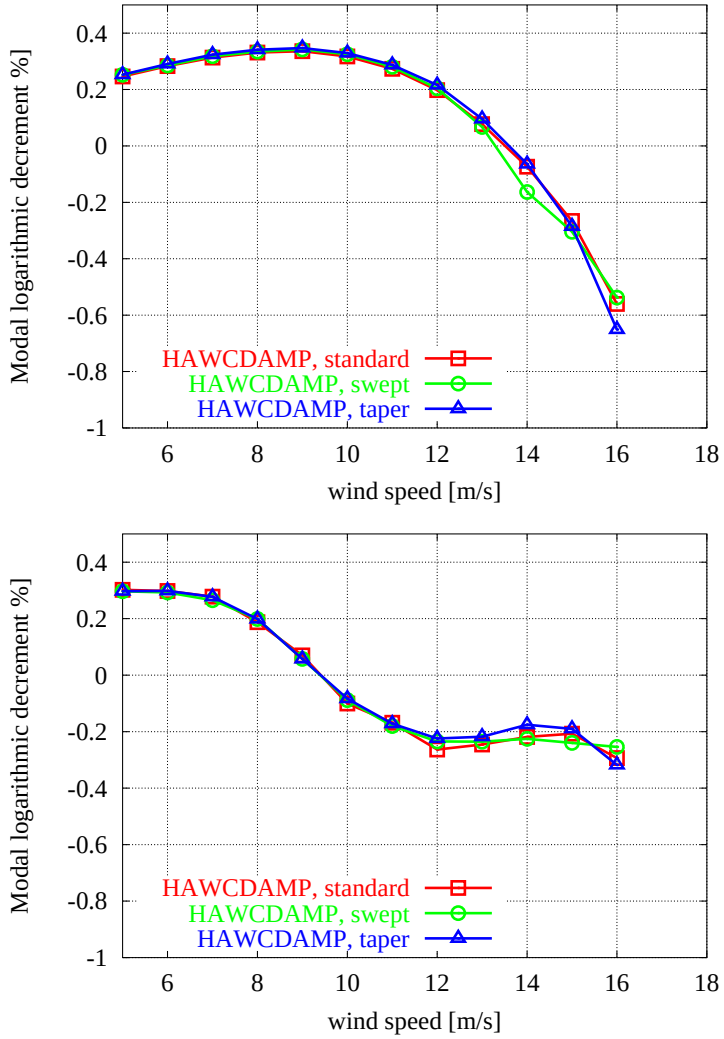

Figure 22: Computations of global modal damping of the three different tips excited in first edgewise mode shape using HAWCDAMP with Stig Øye model (top) and Beddoes-Leishman model (bottom). Only the outer 3.5 m is shown.

Again by looking at the radial distribution of the local modal damping, Figure 23, it is seen that negative local modal damping at the outer 1.5 – 2.5 m of the blade causes the negative damping at wind speeds above 13 m/s.

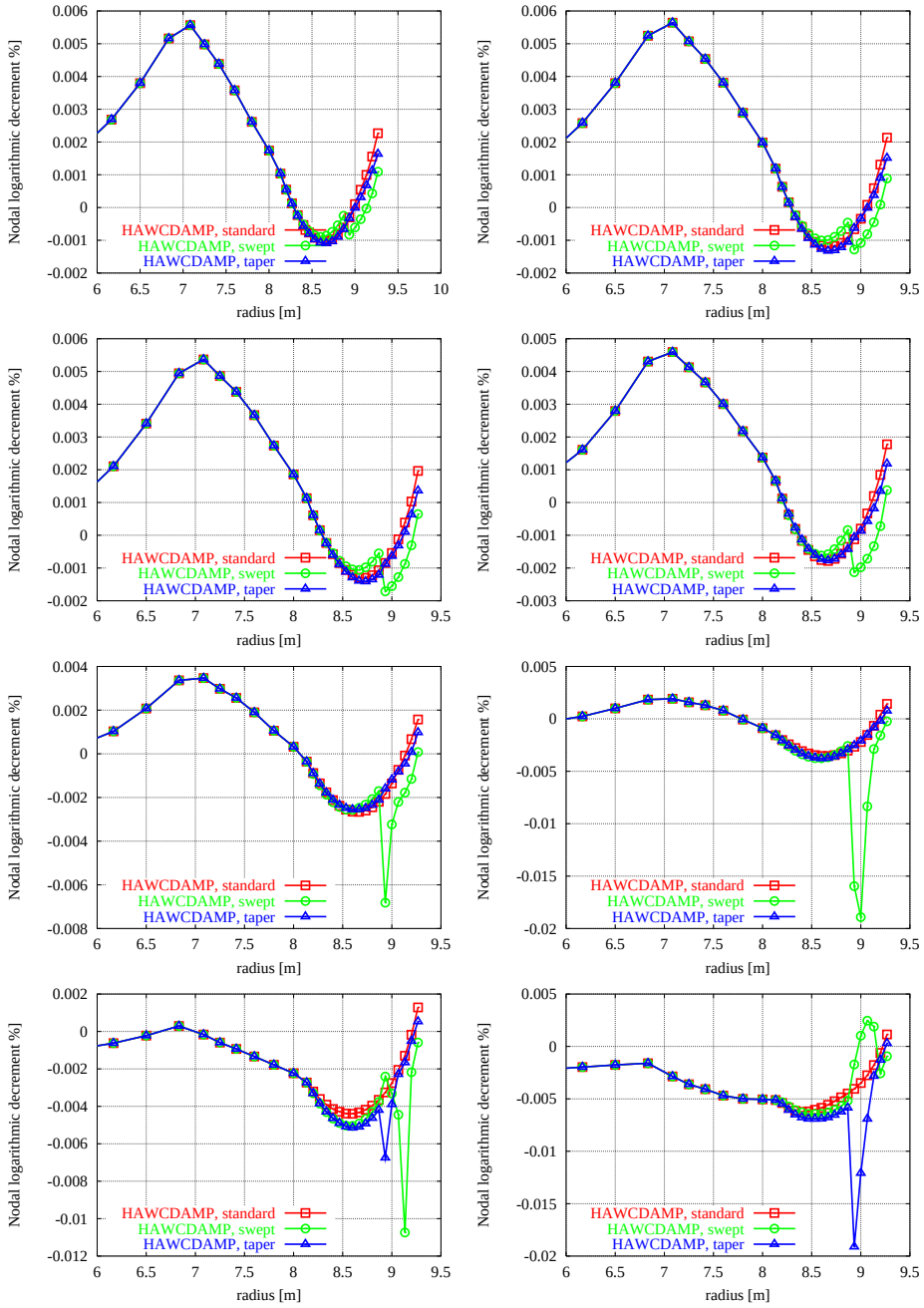

Figure 23: Local modal damping for 9, 10, 11, 12, 13, 14, 15 and 16 m/s, respectively, when first edgewise mode shape is excited. (Stig Øye model).

Discussion

With respect to the flapwise vibrations the Swept tip seems to be slightly less stable compared to the two other tips, even though the level of aerodynamic damping is very high. But with respect to the edgewise vibrations no large difference is observed on the global modal damping.

4 Conclusions

An investigation of the complex three-dimensional flow around the tip of a rotating wind turbine blade using Computational Fluid Dynamics has been performed. Differences in production, flapwise bending moments and radial forces have been investigated and discussed, and flow visualization is used for further analysis. A method for determining the local inflow angle of attack based on the reduction of axial flow velocity has been presented and further analysis is performed on lift and drag coefficients. Three wind speeds below peak power were analyzed. It was shown that the original Standard tip resulted in a more concentrated tip vortex leading to a steeper gradient on both tangential and normal force when approaching the tip, whereas the Swept tip and the Taper tip showed a more flat behavior. At 12 m/s the Swept tip showed a separation pattern on the surface, leading to a steeper gradient in force distributions. The Taper tip keeps the higher loading causing the flapwise bending moment to be higher as seen in the measurements.

To determine the radial variation of lift and drag coefficients the local inflow angle of attack was determined and showed that the Standard tip experienced a slightly larger angle of attack compared to the two tapered tips. At 12 m/s, though, the Swept tip experienced an increase in angle of attack compared to the Taper tip due to a separation at the tip.

The lift coefficients for the Standard tip decreased approaching the tip, while the two tapered tips kept at a more constant lift level. The drag coefficients actually decreased for the two tapered tips, and even becomes negative for the Swept tip. At 12 m/s both lift and drag coefficients changed considerably for the Swept tip due to the separation.

The differences of the aerodynamic damping of the three tips were investigated using HAWCDAMP. The Standard tip seems to be slightly less damped with respect to the flapwise vibrations, but no particular differences were obtained with respect to the edgewise vibrations.

The present study has investigated the very complex flow around a tip of a rotating wind turbine blade. Preliminary conclusions are drawn and further investigations will be carried out before any final conclusions can be drawn with respect to tip design guidelines.

Acknowledgements

The work was funded by the Danish Energy Agency (ENS 1363/01-0001, 'Program for research in aeroelasticity 2001-2002'). Computations were made possible by the use of the IBM RS/6000 SP Power 3 at the Risø central computing facility.

References

[1] Petersen J.T., Madsen H.A., Björck A., Enevoldsen P., Øye S., Ganander H., Winkelaar D. (1998), "Prediction of Dynamic Loads and Induced Vibrations in Stall", Risø Report Risø-I-1045(EN), May 1998

[2] Braun K.A., Arnold H., Gordner A., Hailer F., Huurdeman B., Müller M. (1996) "Some Blade Tip Modifications and their Influence on Aeroacoustics"1996 European Union Wind Energy Conference, 20-24 May, 1996, Göteborg, Sweden.

[3] Antoniou I., Madsen H.A. Paulsen U. S. (1995), "Influence of the tip Shape on the Aerodynamic Behavior of a Wind Turbine Rotor",Risø Report Risø-I-910(EN), December 1995

[4] Michelsen J.A. "Basis3D - a Platform for Development of Multiblock PDE Solvers", Technical Report AFM 92-05, Technical University of Denmark, 1992.

[5] Michelsen J.A. "Block structured Multigrid solution of 2D and 3D elliptic PDE's." Technical Report AFM 94-06, Technical University of Denmark, 1994.

[6] Sørensen N.N. "General Purpose Flow Solver Applied to Flow over Hills." Risø-R-827-(EN), Risø National Laboratory, Roskilde, Denmark, June 1995.

[7] Menter F.R. "Zonal Two Equation k-ω Turbulence Models for Aerodynamic Flows". AIAA-93-2906, 1993.

[8] Thomsen K., Petersen J.T. "HAWCDAMP v. 1.0 – beregning af aerodynamisk dæmpning". Risø National Laboratory, 2000.

Bibliographic Data Sheet **Risø-R-1353(EN)**

Title and authors

Numerical Investigation of Three Wind Turbine Blade Tips

Jeppe Johansen, Niels N. Sørensen

ISBN	ISSN
87-550-3087-4 87-550-3088-2(Internet)	0106-2840

Department or group	Date
Wind Energy Department	August 2002

Groups own reg. number(s)	Project/contract No(s)
	Program for research in aeroelasticity 2001-2002/ ENS 1363/01-0001

Pages	Tables	Illustrations	References
27	1	23	8

Abstract (max. 2000 characters)

The complex three-dimensional flow around three different tip shapes on a rotating wind turbine blade is investigated and analyzed using Computational Fluid Dynamics. Differences in production, flapwise bending moments and forces are discussed. A method for determining the local inflow angle of attack is presented and further analysis is performed on lift and drag coefficients.

It is shown that the original Standard tip results in a more concentrated tip vortex leading to a steeper gradient on both tangential and normal forces when approaching the tip, whereas the two tapered tips show a more flat behavior. This again leads to lower flapwise bending moments and lower production for the Standard tip compared to the two tapered tips. At 12 m/s, though, the Swept tip shows a separation pattern on the surface. This separation causes a decrease in normal force and an increase in tangential force. The Taper tip keeps the higher loading causing the flapwise bending moment to be higher as seen in measurements.

To determine the radial variation of lift and drag coefficients the local inflow angle of attack is determined. It is shown that the Standard tip experiences a slightly larger angle of attack at the tip compared to the two tapered tips. The lift coefficients are kept at a more constant level for the two tapered tips due to the decrease in chord, while the drag coefficients actually decrease for the two tapered tips, especially for the Swept tip. For the Swept tip at 12 m/s both lift and drag coefficients changed considerably due to the separation

Differences in aerodynamic damping of the three tips were investigated using HAWCDAMP. The Standard tip seems to be slightly less damped with respect to the edgewise vibrations.

Descriptors INIS/EDB

AERODYNAMICS; COMPUTATIONAL FLUID DYNAMICS; NAVIER-STOKES EQUATIONS; TURBINE BLADES; WIND TURBINES